Low Temperature Physics/Fizika Nizkikh Temperatur, 2017, v. 43, No. 7, pp. 1037–1045

From single SQUID to superconducting quantum arrays

V.K. Kornev and N.V. Kolotinskiy

Faculty of Physics, Lomonosov Moscow State University, Moscow 119991, Russia
E-mail: kornev@phys.msu.ru

A.V. Sharafiev

Institution of Quantum Optics and Quantum Information, Innsbruck 6020, Austria

I.I. Soloviev

Skobeltsyn Institute of Nuclear Physics, Lomonosov Moscow State University, Moscow 119991, Russia

O.A. Mukhanov

HYPRES, Inc., 175 Clearbrook Road, Elmsford, NY 10523, USA

Received February 7, 2017, published online May 25, 2017

Superconducting quantum arrays (SQAs) capable of providing highly linear voltage response to magnetic signal and high dynamic range have been suggested and developed. Base elements of the arrays, quantum cells, were devised and studied in detail. Using niobium process, SQAs with different number of the cells and prototypes of the SQA-based broadband active electrically small antennas were fabricated and tested.

PACS: **85.25.–j** Superconducting devices;
85.25.Dq Superconducting quantum interference devices (SQUIDs);
85.25.Cp Josephson devices.

Keywords: Josephson junctions, SQUID, superconducting quantum arrays, quantum cells, linearity, dynamic range, broadband devices.

Introduction

DC SQUIDs are known and widely used as extremely sensitive amplifiers [1,2], but showing only limited linearity voltage response. In conventional low-frequency SQUID systems, the improved linearity and dynamic range DR are obtained by using an external feedback loop, which has limited bandwidth (not exceeding 1 MHz). Such an external feedback approach is unfeasible in case one needs to design a SQUID-based system with very broad bandwidth. A solution may be found by using Josephson-junction array structures. Term “superconducting quantum arrays” (SQAs) has been recently suggested to denote the special arrays designed to achieve both highly linear magnetic signal to voltage transfer function and high dynamic range [3].

Integrating such a SQA with a broadband input line to apply an input magnetic signal to all array cells (see, for example, the designs proposed in [4,5]), one can design a high-performance broadband amplifier. Moreover, an active electrically small antenna (ESA) can be developed on the basis of SQA to implement simultaneously broadband reception and amplification of electromagnetic signals. Practical implementation of these active ESAs is significantly simplified due to the absence of input RF line (e.g. see designs used in [6–8]). When integrated with a superconducting transformer (concentrator) of magnetic flux, SQA can function as active ESAs of transformer type [9–11]. At the same time, the 2D SQAs with nonsuperconducting electric connection of the superconducting cells can be used directly as active ESAs of a transformer-less type [11].

In this paper, we summarize our theoretical and experimental studies aimed at the development of high-efficiency SQAs and SQA-based devices.

Superconducting quantum array concept

SQA is a uniform periodic structure composed of identical superconducting cells with a linear voltage response to applied magnetic signal [3]. These cells are electrically

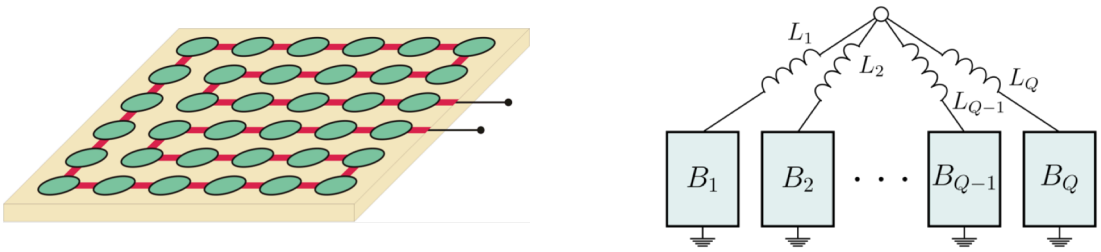

(a) (b)

Fig. 1. Schematic of (a) SQA and (b) SQA composed of K_P blocks "*B*" connected in parallel each consisting of K_S Superconducting Quantum Cells (SQC) connected in series. L_1, L_2, ... L_Q are coupling inductances. In general case, the blocks B_k may be serial arrays of sub-blocks each having structure like the presented structure of SQA.

connected in series or parallel-series into a 2D array (shown schematically in Fig. 1(a)) or can be arranged into a 3D multi-chip configuration. SQA is characterized by independent operation of individual cells and collective behavior of an entire array generating an output signal. The dynamic range of the linear output signal increases with the number of cells N proportionally to $\sqrt{N}$. In fact, in view of the independence of fluctuations of the cell output voltage, the spectral density of low-frequency (at the signal frequency) fluctuations of the circuit output voltage for cells connected in series is $S_V(0) = NS_V^0(0)$, where $S_V^0(0)$ is the spectral density of low-frequency fluctuations of the output voltage of one cell. Thus, the *rms* output signal fluctuations $V_F = [NS_V^0(0)]^{1/2}$ increase proportionally to $\sqrt{N}$, and the output signal $V(\Phi)$ and conversion factor $dV/d\Phi$ of the applied magnetic flux Φ to voltage V increase proportionally to N. For cells connected in parallel, the output voltage and conversion factor $dV/d\Phi$ do not change, and the spectral density of low frequency current fluctuations increases proportionally to the number of cells: $S_I(0) = NS_I^0(0)$, where $S_I^0(0)$ is the spectral density of independent sources of fluctuation currents connected to the cells in correspondence with the Langevin method [12–14]. Therefore, the *rms* value of output signal fluctuations $V_F = [NS_I^0(0)]^{1/2} R_d/N$, where R_d is the differential resistance at the operation point of the current−voltage characteristic (*I*–*V* curve) of the superconducting cell, decreases as $N^{-1/2}$. In both cases, the *rms* fluctuations reduced to the input of one cell, $V_F(dV/d\Phi)^{-1}$, decrease with an increase in the number of cells N as $1/\sqrt{N}$.

A proper serial-parallel cell connection pattern can be used to set impedance of the array in compliance with application conditions. For simplicity, one may assume that SQA is composed of K_P blocks "*B*" connected in parallel each consisting of K_S cells connected in series as shown schematically in Fig. 1(b). In this configuration, the normal resistance of the array is expressed through normal resistance R_N of one cell:

$$R_{NA} = R_N K_S / K_P. \tag{1}$$

At the same time, total number of the cells $N = K_S K_P$ determines the dynamic range achievable for the SQA-based device [3]:

$$DR = (K_S K_P)^{1/2} DR_1, \tag{2}$$

where DR_1 is dynamic range of single cell. One should note, that relation (2) holds only in the case when impedance ΩL of the coupling inductances L_k between the blocks "B" at signal frequency is much less than the normal resistance of the blocks $K_S R_N$.

Cells of superconducting quantum arrays

Two Josephson-junction circuits, a bi-SQUID [15–17] and a differential circuit cell [17–20], were suggested to be used as superconducting quantum cells (SQC). Bi-SQUID is a circuit composed of rf and dc SQUID loops as shown in Fig. 2(a). This device can provide a high-linearity voltage response to the applied magnetic flux Φ_e, when a proper critical current value I_{c3} is assigned to the third Josephson junction *J*3 [21,22]. Figure 2(b) shows the highly linear response, which is triangular at $l \sim 1$ and hysteretic at $l > 1$, where $l = 2\pi I_c L_{rf}/\Phi_0$ is normalized value of the rf SQUID loop inductance L_{rf}, I_c is critical current of the dc SQUID-loop junctions *J*1 and *J*2, $\Phi_0 = h/2e$ (h is Plank constants, and e is electron charge) is magnetic flux quantum. The response linearity can peak up to 90 dB (and even more) [21] at optimally set I_{c3} when taking into account all values of the device inductances — inductances L_{rf} and L_{dc} of rf and dc SQUID loops, as well as a shared inductance L_m of the loops (not shown in Fig. 2(a)) [21]. Optimal values of $i_{c3} \equiv I_{c3}/I_c$ are presented in Fig. 3 as $l_{dc} = 2\pi I_c L_{dc}/\Phi_0$ versus $l^* = li_{c3} \equiv 2\pi I_{c3} L_{rf}/\Phi_0$, when inductance L_m is assumed vanishing.

Numerical value of the device linearity can be introduced through a standard single-tone analysis technique as follows. When applying sinusoidal input signal, the device linearity is derived with formula $Lin = b_1/\max\{b_k\}$, where b_1 and b_k are the amplitudes of basic tone and harmonic components of the output signal.

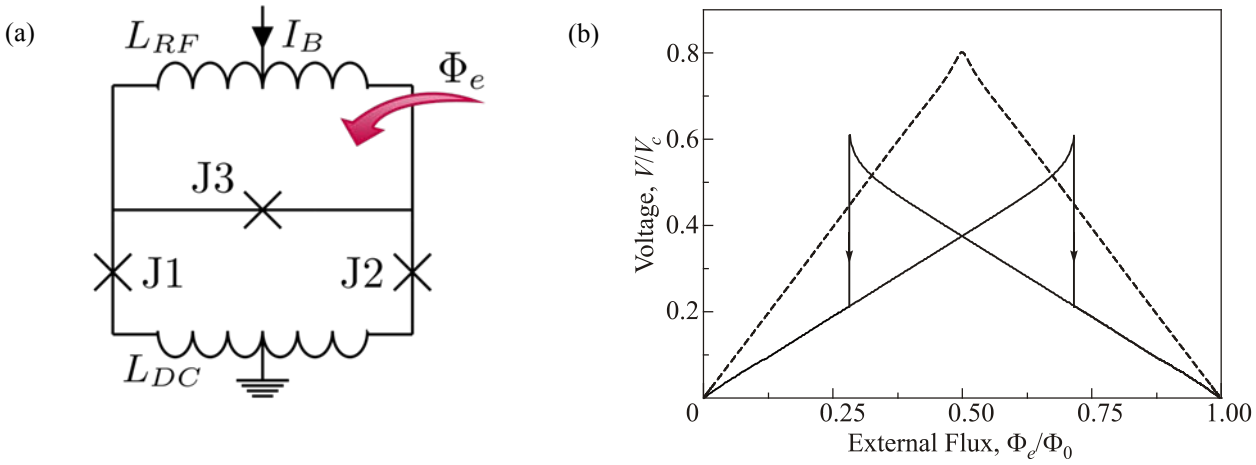

Fig. 2. (a) Equivalent circuit of bi-SQUID and (b) its linear voltage response at $l = 1$, $i_{c3} \equiv I_{c3}/I_c = 1.0$ (dash line) and $l = 4$, $i_{c3} = 0.76$ (solid line); bias current $I_b = 2I_c$, where I_c is critical current of Josephson junctions $J1$ and $J2$ in the dc SQUID loop, I_{c3} is critical current of the third junction, $l = 2\pi I_c L/\Phi_0$ is normalized value of the rf SQUID loop inductance L_{rf}, and inductance L_{dc} of the dc SQUID loop is considered negligibly small.

In practice, one should also take into account thermal noise and spread in critical currents [23]. The noise impact increases with factor $\gamma = 2ek_BT/\hbar I_c$ (here T is ambient temperature, k_B & $\hbar$ are Boltzmann and Plank constants) and smoothens corners of the cell response and reduces its linear part. The spread in critical currents results in both the departure of l^* from its optimal value and different biasing $I_b/2I_c$ of the cells connected in series (see also [24] where non-uniform arrays are considered). These factors, at first place the multi-parameter (L_{rf}, L_{dc}, L_m) dependence of the response linearity, impedes the implementation of the bi-SQUIDs as basic cells of the SQAs.

Figure 4(a) shows schematically DQC and a serial array of DQCs. The cell is composed of two differentially connected parallel arrays each of n Josephson junctions coupled via substantially low inductances L_a. The cell arms are

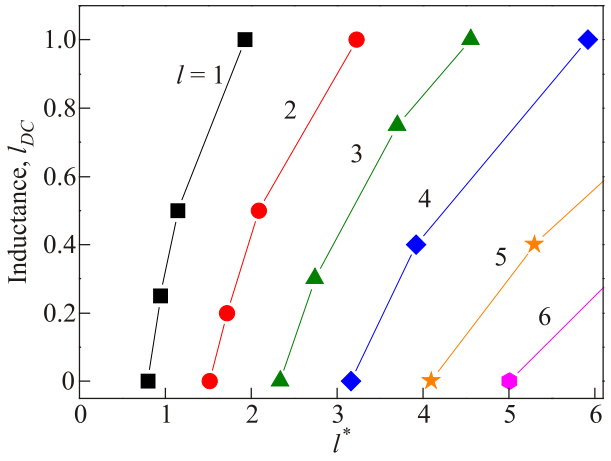

Fig. 3. Optimal values of $i_{c3} \equiv I_{c3}/I_c$ as $l^* = li_{c3}$ vs, $l_{dc} = 2\pi I_c L_{DC}/\Phi_0$ for $l = 1$, 2, 3, and 4, when shared inductance L_m is assumed vanishing.

to be oppositely biased by some magnetic flux Φ_b. Each of the arms should be biased with a dc current $I_b \approx nI_c$, where I_c is Josephson junction critical current, and the same input magnetic flux signal Φ_{in} must be applied to both arms. When composed of DQCs, the SQA in fact consists of two differentially connected arrays of left and right arms of the cells. Figure 2(b) shows a typical voltage response of such a differential cell as well as responses of the cell arms; the response linearity can exceed 100 dB [25].

The increase in the number n of Josephson junctions in the DQC arm decreases impedance (normal resistance) of the cell and increases its dynamic range as $\sqrt{n}$. However, the latter keeps on only at the low coupling impedances between all the junctions $k\Omega L_a$ ($k \le n$) as compared to the junction normal resistance, i.e. up to $n\omega l_a \sim 1$, where $l_a = 2\pi I_c L_a/\Phi_0$, and ω is signal frequency Ω normalized to the characteristic Josephson-junction frequency $\Omega_c = 2\pi I_c R_N/\Phi_0$.

Figure 5 shows linearity of the DQC voltage response versus magnetic bias Φ_b of the 20-junction arms of the differential cell with coupling inductances $l_a = 0.5$, calculated for different amplitudes of the input magnetic signal Φ_{in} when the signal exploits 50% (solid line) and 30% (dash line) of the total response swing. The linearity peak position Φ_{opt} shows weak dependence on the coupling inductance: $\Phi_{opt} \simeq 2.20\Phi_0$, $2.48\Phi_0$, $2.98\Phi_0$ ($0.115\Phi_0$, $0.138\Phi_0$, $0.159\Phi_0$ per elementary loop) at $l_a = 0.5$, 0.7, 0.8, respectively. This shift in Φ_{opt} with l_a follows from some small changes in the response form with change in an effective interaction "radius" (can be characterized by number k of the junctions within the radius) at Josephson-oscillation frequency Ω_j in compliance with the voltages V_1 and V_2 across the cell arms (the frequency relationship is to be as follows: $\Omega << \Omega_j \lesssim \Omega_c$).

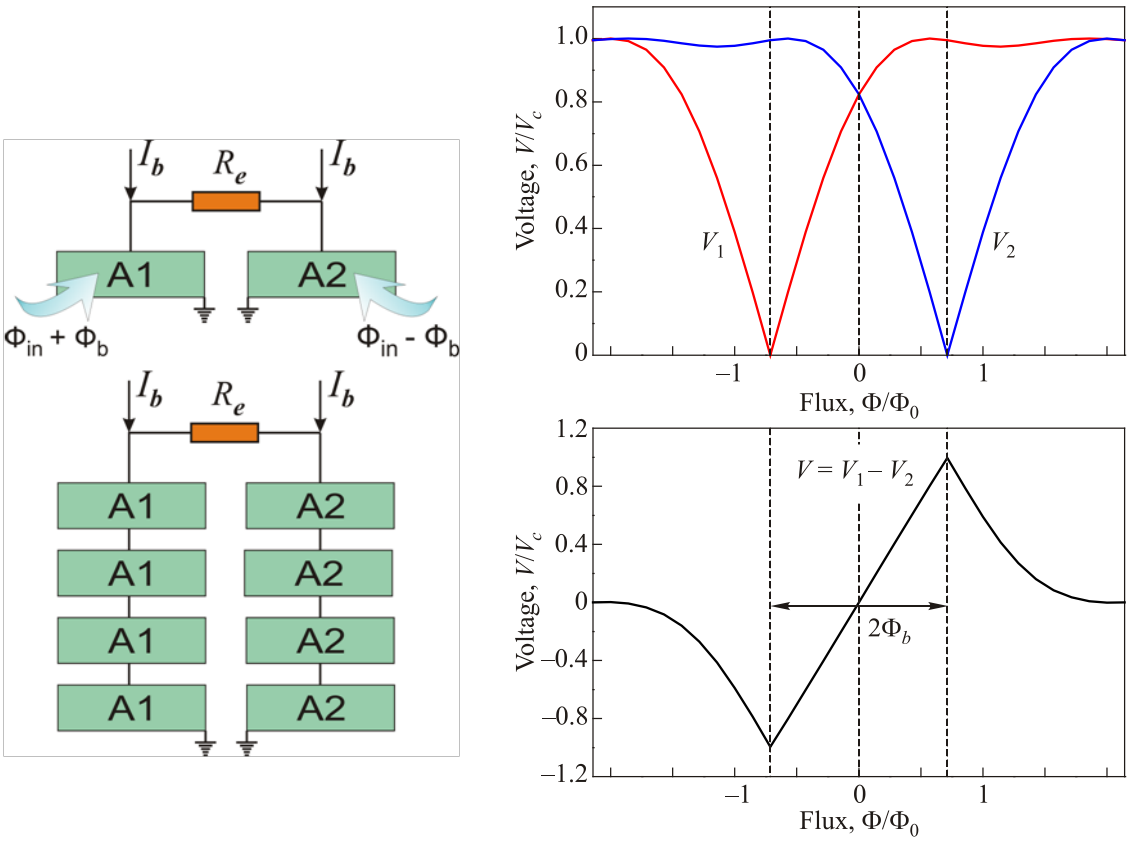

(a) (b)

Fig. 4. (Color online) (a) Schematic of differential quantum cell (DQC) consisting of two parallel Josephson-junction arrays $A1$ and $A2$ of n junctions (top). Serial DQC array (bottom); R_e is external load, I_b is bias current. (b) Voltage responses of the cell arms (top) at $I_b = nI_c$ (critical current of the arms) and resulting response of the cell (bottom).

In practice, this cell was found much more convenient for the design and implementation of an SQA as compared to bi-SQUID cell.

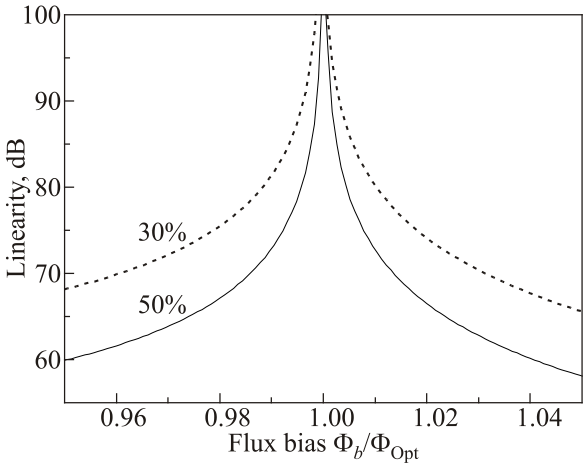

Fig. 5. Dependence of the voltage response linearity on the flux biasing Φ_b of the cell arms when the applied input signal exploits 50% (solid line) and 30% (dash line) of the total response swing. Φ_{opt} is flux bias answering maximum linearity. The cell arms are parallel arrays of 20 Josephson junctions. Normalized value of the coupling inductances $l_a = 0.5$.

Matching issues of SQAs

The SQA-based device is a two-terminal active network with the output and bias in one port (in case of the DQC-based arrays, ground terminal plays only an ancillary role and therefore is left out of account). Therefore, in contrast to conventional passive devices, SQA ought to be strongly mismatched with the connected load to maintain the high linearity of the voltage output [25]. In case of differential quantum cells, the linearity can be nearly balanced with some increase in the bias current (within about 6% increase), when the load impedance R_e is about ten to fifteen times higher than the SQA impedance R_N (normal resistance of SQA). The desired impedance of SQA can be set using a proper serial-parallel connection pattern for the quantum cells. In spite of the required strong mismatching, the SQA-based devices are capable of providing a quite high output power P_{out} at the expense of bias current supply. In fact, $P_{out} = I_e V_{out} / 2$, where I_e is the output current amplitude (up to about 5% of the bias current I_b) and V_{out} is the output voltage amplitude which is proportional to the number K_s of the quantum cells connected in series. When delivering output signal to a low-impedance (of order of a few Ohms) device such as superconductor analog-to-

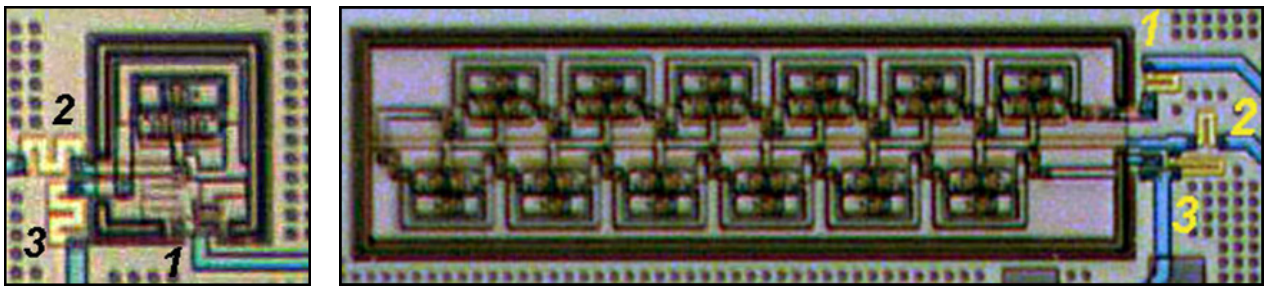

(a) (b)

Fig. 6. (Color online) Microphotographs of (a) single bi-SQUID and (b) array of 12 bi-SQUIDs connected in series. Black dots and bold black lines around the devices are holes in a superconductor ground layer (light background) used for flux trapping protection Lines "*1*" and "*2*" are to apply bias current I_b and measure voltage across the circuits, which are two-terminal devices with one terminal connected to the ground layer. Line "*3*" is connected to a grounded control line, which is inductively coupled with the input bi-SQUID loops for application of magnetic flux signal.

digital converter (ADC), a broadband superconducting impedance transformer can be used to match interface and prevent a standing wave formation.

Experimental research

To perform experimental study, multiple arrays of bi-SQUIDs and differential quantum cells connected in series as well as a number of SQAs were fabricated using niobium process with critical current density j_c = 4.5 kA/cm^2 [26]. For the most part, Josephson junction critical current value I_c was set as 125 μA. The tunnel junctions were *in situ* shunted with a sufficiently low resistor (playing role of normal resistor R_N of the junctions) to decrease McCumber parameter $\beta = 2\pi I_c R_N^2 C$ down to 0.2 to 0.1, when the impact of the junction capacitance C on the device characteristics becomes negligibly small. All measurements were performed at temperature 4.2 K.

Bi-SQUID arrays

Figure 6 shows microphotographs of a single bi-SQUID and an array of 12 bi-SQUIDs connected in series. Black dots and bold black lines around the devices are holes in superconductor ground layer (light background), both are meant for protection against flux trapping. Magnetic signal was applied using control line (started from connecting line "*1*" and terminated to the ground layer) inductively coupled with the input bi-SQUID loops. This stripline goes just over the loop striplines separated by an insulator layer of about 150 nm thickness.

As an example, two sets of the experimentally measured voltage responses of the serial arrays of bi-SQUIDs with bias current I_b are presented in Fig. 7. The first set (at l = 0.85 and i_{c3} = 1.2) was obtained with parameter values corresponding to a triangular response shape which

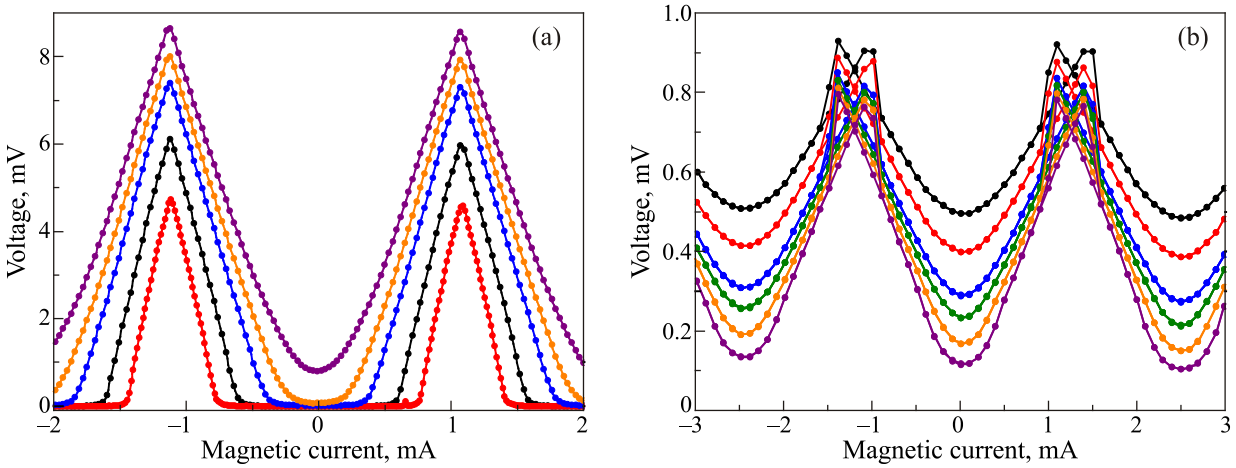

Fig. 7. (Color online) Sets of voltage responses of the serial arrays of (a) 128 bi-SQUIDs (l = 0.85, i_{c3} = 1.2) and (b) 20 bi-SQUIDs (l = 2.5, i_{c3} = 0.8) with bias current I_b starting (bottom curve) with a magnitude less than $2I_c$ (of about $0.6{\cdot}2I_c$) (a) and with a magnitude 2% higher than $2I_c$ (b).

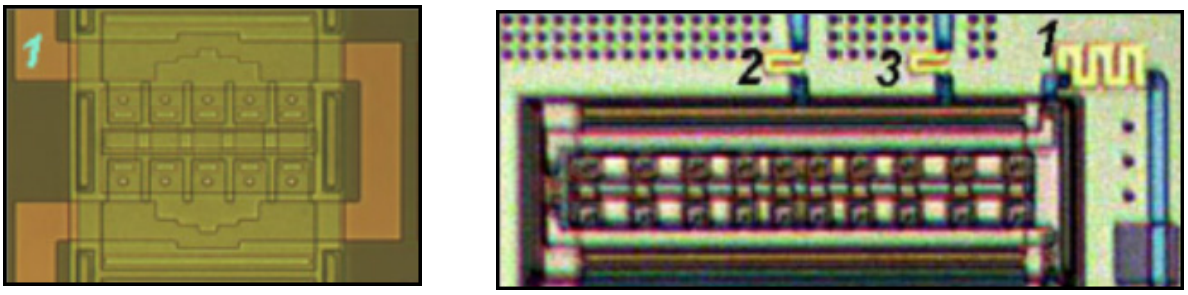

(a) (b)

Fig. 8. (Color online) Microphotographs of two base units of serial arrays of the differential quantum cell arms: (a) a pair of 5-junction parallel arrays connected in series top-down and (b) a pair of 10-junction parallel arrays connected in series top-down. Meander control strip lines "*1*" are to apply both the magnetic flux signal and flux bias. Lines "*2*" and "*3*" in (b) are to apply bias current and measure voltage across the array, respectively.

is optimal at $l \leq 1$. The second set ($l = 2.5$, $i_{c3} = 0.8$) was obtained with parameter values close to the optimal ones at $l > 1$. Sharp lower corners as shown in Fig. 2(b), which presents theoretical responses of single bi-SQUID at $I_b = 2I_c$, were not observed for the array responses in the presence of critical current spread (of order of 1%) which does not allow the realization of the uniform critical-current biasing of all bi-SQUIDs in the serial array. Instead of the strongly sharp corner, a smoothed corner is observed; the corner becomes less smoothed with some increase in biasing when the bias current exceeds all individual critical currents ($2I_c$) of the array elements (see the upper curve in Fig. 7(a) and curves in Fig. 7(b)). Noise factor γ at $T = 4.2$ K and $I_c \approx 125$ μA is quite low ($\sim 1.4 \cdot 10^{-3}$) and therefore the noise impact is much less than the one of the critical current spread (of order of 1%).

Differential quantum cell arrays

The serial array of the differential quantum cells consists of two serial arrays of the left and right arms of the DQCs (parallel arrays of n Josephson junctions) connected differentially. Each array arm was constructed as a serial array of basic blocks of two parallel arrays with mirror symmetry in their topologies. For example, microphotographs in Fig. 8 presents two basic blocks with $n = 5$ and $n = 10$ junctions in the parallel arrays. The control striplines with a meander shape (lines "*1*") are to apply both the magnetic flux signal and flux bias. To increase magnetic coupling to inductances between Josephson junctions in the parallel array, the control line goes just over the stripline connecting the junctions. The overlapped strip lines are separated by an insulator layer of about 150 nm thickness. Lines "*2*" and "*3*" in Fig. 8(b) are to apply bias current and measure voltage across the arm array (an output voltage), respectively.

To suppress any resonance excitations in the array structures, these blocks were connected in series via small resistors of the order of 0.1 Ohm. Due to these resistors, the superconducting branches in *I–V* curves of the arm arrays have some slope. Fig. 9(a) shows a typical set of *I–V* curves of such a serial array with magnetic flux applied (i.e., with magnetic current in the control line). This array

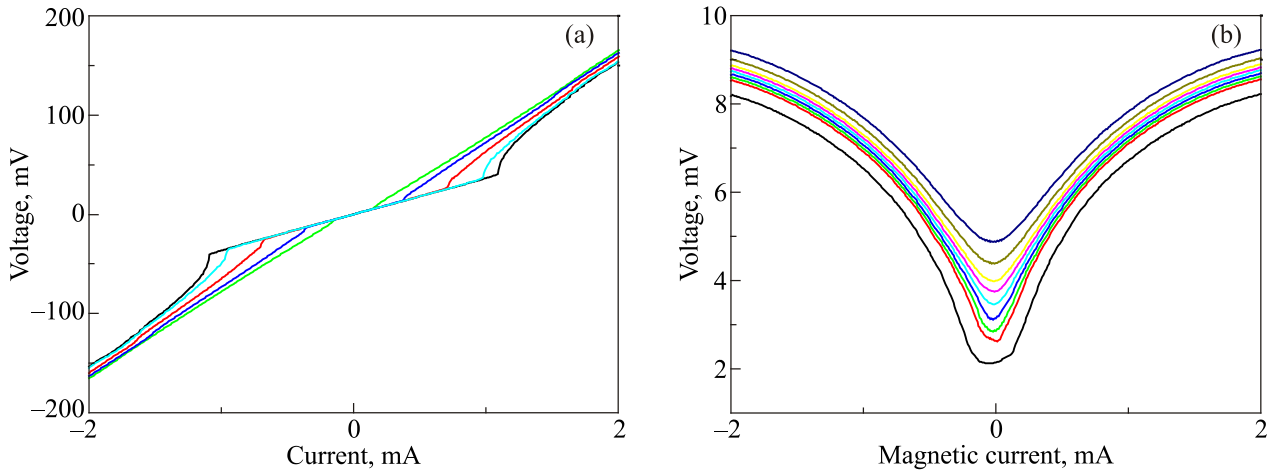

Fig. 9. (Color online) Set of *I–V* curves of the serial array of 400 10-junction arms at different magnetic fluxes applied (a) and set of voltage responses of the serial arrays of 60 12-junction arms with bias current I_b starting (bottom curve) with a magnitude of about $0.96 \cdot 12 I_c$ (b).

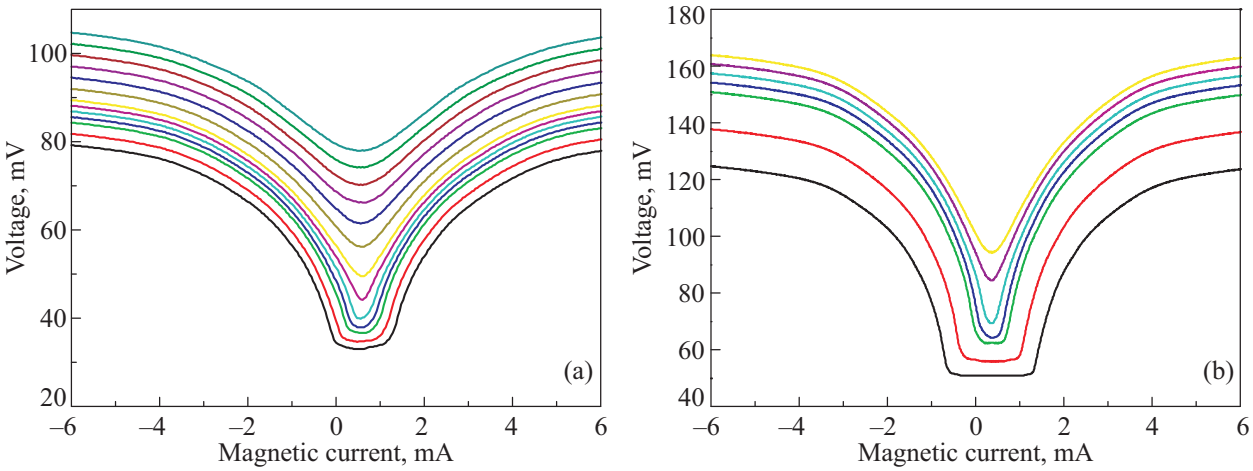

Fig. 10. (Color online) Two sets of the voltage responses of the serial arrays of 408 (a) and 816 (b) 12-junction arms with bias current I_b starting (bottom curves) with magnitudes of about $0.94 \cdot 12 I_c$ (a) and $0.8 \cdot 12 I_c$ (b).

consists of 64 base blocks, each of two 10-junction parallel arrays. Typical set of voltage responses of such array (which is an arm of SQA) with bias current is presented in Fig. 9(b). This array contains 30 basic blocks; each integrates two 12-junction parallel arrays. Figure 10 shows sets of voltage responses with bias current I_b for much longer serial arrays containing 204 (a) and 408 (b) base blocks, each of two 12-junction arrays (n = 12). The responses ought to have a flat anti peak at $I_b < nI_c$ and a slightly roundish response tip at $I_b > nI_c$, while at $I_b = nI_c$ this anti-peak ought to be sharp. However, the sharp tip is not observed as a consequence of the present spread in critical currents within the serial arrays.

Figure 11(a) shows photograph of the chip of 5×5 mm size with the fabricated SQA occupying area of about 3.3×3.3 mm, and Fig. 11(b) presents a set of the experimentally measured voltage responses of this SQA, composed of 408 differential cells, with bias flux Φ_b. The SQA consists of two serial arrays of 12-junction arms (12-junction parallel arrays) of differential cells. Each of the presented SQA voltage responses is a difference of the serial array responses to the applied magnetic flux when these responses are oppositely shifted by the bias flux Φ_b. Both the input magnetic flux and bias flux were applied using a control line inductively coupled with the differential cell arms.

Discussion

A number of SQAs with different number of the differential cells and various topologies of the cells and control lines, including prototypes of the SQA-based active ESA of both transformer and transformer-less types, were fabricated and tested. In particular, a prototype of SQA-based ESA composed of 560 cells demonstrated peak-to-peak volt-

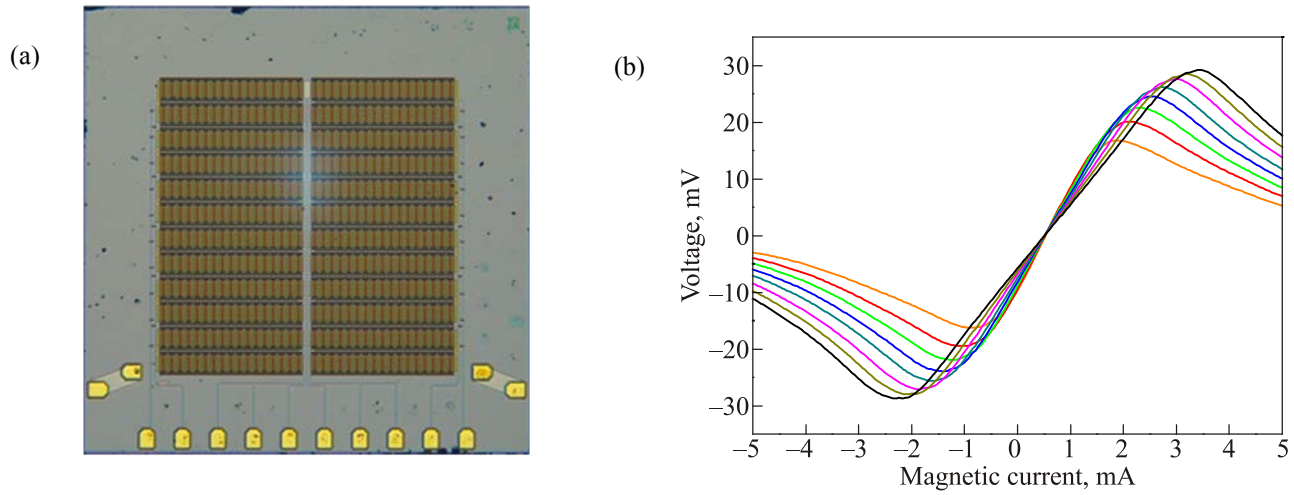

Fig. 11. (a) Photograph of the chip of 5×5 mm size with the fabricated SQA of 408 differential cells. The SQA occupies area of about 3.3×3.3 mm. (b) Set of the SQA voltage responses to the magnetic flux, applied using control line current, with the flux biasing Φ_b of the SQA arms (each of 12 Josephson junctions).

age response of about 80 mV and the steepness dV/dB of the magnetic signal conversion into output voltage of about 6500 μV/μT [11], when the input magnetic signal was applied using an external multi-turn coil. As for linearity of the SQA output signal, our measurements demonstrated linearity up to 70 dB [11]; a higher linearity could not be reliably observed with the employed measurement setup. We used a well-known two-tone analysis technique by applying two sinusoidal input signals with equal amplitudes and close frequencies $\omega_1 \sim \omega_2$. The resultant device linearity was derived using formula $Lin = b / \max\{b_{km}\}$, where b and b_{km} are amplitudes of these signals and intermodulation components (at frequencies $k\omega_1 \pm m\omega_2$) in the output signal, respectively. This was measured at signal frequency of 300 kHz within ~30% to ~80% of the linear region of the voltage response.

In spite of the low frequency used in the measurements, the results can be adequately translated to much higher frequencies up to about ten GHz (and even higher) [20] under a condition that the frequency remains much less than Josephson oscillation frequency. Small size of the antenna as compared to the wavelength makes it a lumped element, excluding any distributed element effects. As for other parasitic effects, which can be at higher frequencies (e.g. resonances), their existence manifests itself through peculiarities in the I–V curve, and therefore the effects can be found with simple dc measurements.

Prototypes of the SQA-based antennas were tested applying magnetic field using both the on-chip strip coil and external multi-turn coil. In the latter case, no magnetic shielding was used, except exterior μ-metal can outside of Dewar liquid Helium vessel. This gives about ten times reduction of the Earth magnetic field. Both the same shielding and additional shielding with two mutually embedded μ-metal cans around the chip were used in the measurements with on-chip strip coil. No essential difference was observed in the tests. Moreover, the evidence of operating capability of such superconducting antennas in unshielded environment follows from the experiments in which some similar superconducting array structures were used successfully as antennas to receive both the near field and far field signals [6–8].

Both the transformer (superconducting flux concentrator) and transformer-less active ESAs can be implemented delivering high performance. Having the same area, a transformer-less ESA can integrate larger number of the quantum cells and therefore can have a higher dynamic range. At the same time, such an antenna can suffer from some dimensional effects, restricting the attainability of the highest linearity for certain directions [27,28]. Transformer-type antennas can be free from any dimensional effects and may have even higher sensitivity in spite of the lower output signal and lower dynamic range due to the lower number of the basic cells [27,28].

Conclusion

Superconducting quantum arrays have been proposed, developed, fabricated using niobium process, and tested. These arrays are of a great importance for the implementation of highly sensitive broadband devices with high spurious-free dynamic range unachievable with single SQUIDs. Two types of quantum cells with linear voltage response to magnetic signal were proposed as basic elements for SQAs, namely, bi-SQUID and the DQC. The latter delivered better performance for SQAs.

The SQAs can be used as front-end circuits for broadband radio frequency systems such as broadband receiving systems with direct digitization of input signal [29–35] for various applications including broadband communications, radar, surveillance, etc. One can mention broadband low-noise amplifiers (e.g., see design approaches in [4,5]) as well as broadband active electrically small antennas (ESAs) capable of providing concurrent receiving and amplification of the broadband electromagnetic signals. The SQAs are also beneficial for many applications, in which SQUIDs and SQUID arrays are being used [1,2,36].

One should note also that the expected progress in Josephson junction fabrication technology, e.g., with a further increase in critical current density of the niobium process or with advancement in high-temperature superconductor technology [37–39], will allow improving characteristics of the quantum cells and hence the SQA-based devices.

1. R. Kleiner, D. Koelle, F. Ludwig, and J. Clarke, *Proc. IEEE* **92**, 1534 (2004).
2. R.L. Fagaly, *Rev. Sci. Instrum*. **77**, 101101 (2006).
3. V.K. Kornev, A.V. Sharafiev, I.I. Soloviev, N.V. Kolotinskiy, V.A. Skripka, and O.A. Mukhanov, *IEEE Trans. Appl. Supercond.* **24**, 1800606 (2014).
4. G.V. Prokopenko, O.A. Mukhanov, A. Leese de Escobar, B. Taylor, M.C. De Andrade, S. Berggren, P. Longhini, A. Palacios, M. Nisenoff, and Robert L. Fagaly, *IEEE Trans. Appl. Supercond.* **23**, 1400607 (2013).
5. S. Berggren, G. Prokopenko, P. Longhini, A. Palacios, O.A. Mukhanov, A. Leese de Escobar, B.J. Taylor, M.C. de Andrade, M. Nisenoff, R.L. Fagaly, T. Wong, E. Cho, E. Wong, and V. In., *IEEE Trans. Appl. Supercond*. **23**, 1400208 (2013).
6. O.A. Mukhanov, G.V. Prokopenko, and R. Romanofsky, *IEEE Microw. Mag*. **15**, 57 (2014).
7. M.C. de Andrade, A. Leese de Escobar, B.J. Taylor, S. Berggren, B. Higa, S. Dinh, R.L. Fagaly, J. Talvacchio, B. Nechay, and J. Przybysz, *IEEE Trans. Appl. Supercond*. **25**, 1603005 (2015).
8. G.V. Prokopenko, O.A. Mukhanov, and R.R. Romanofsky, *2015 IEEE 15th Int. Supercond. Electron. Conf. (ISEC), 6–9 July* (2015).
9. V.K. Kornev, I.I. Soloviev, N.V. Klenov, A.V. Sharafiev, and O.A. Mukhanov, *IEEE Trans. Appl. Supercond*. **21**, 713 (2011).

10. V. Kornev, I. Soloviev, N. Klenov, A. Sharafiev, and O.A. Mukhanov, *Physica C* **479**, 119 (2012).
11. V.K. Kornev, I.I. Soloviev, A.V. Sharafiev, N.V. Klenov, and O.A. Mukhanov, *IEEE Trans. Appl. Supercond*. **23**, 1800405 (2013).
12. K.K. Likharev, *Dynamics of Josephson Junctions and Circuits*, Gordon and Breach, New York (1985).
13. R.L. Stratonovich, *Selected Topics in the Theory of Random Noise*, Gordon and Breach, New York (1967).
14. A.D. Whalen, *Detection of Signals in Noise*, Academic, New York (1971).
15. V.K. Kornev, I.I. Soloviev, N.V. Klenov, and O.A. Mukhanov, *Supercond. Sci. Tech*. **22**, 114011 (2009).
16. V.K. Kornev, I.I. Soloviev, N.V. Klenov, A.V. Sharafiev, and O.A. Mukhanov, *IEEE Trans. Appl. Supercond.* **21**, 713 (2011).
17. V.K. Kornev, I.I. Soloviev, N.V. Klenov, and O.A. Mukhanov, *Physica C* **470** 886 (2010).
18. V.K. Kornev, I.I. Soloviev, N.V. Klenov, and O.A. Mukhanov, *IEEE Trans. Appl. Supercond.* **19**, 741 (2009).
19. V. Kornev, N. Kolotinskiy, V. Skripka, A. Sharafiev, I. Soloviev, and O. Mukhanov, *J. Phys.: Confer. Ser.* **507**, 042018 (2014).
20. V. Kornev, A. Sharafiev, N. Kolotinskiy, and O. Mukhanov, *IEEE Trans. Appl. Supercond*. **25**, 1602306 (2015).
21. V.K. Kornev, N.V. Kolotinskiy, D.E. Bazulin, and O.A. Mukhanov, *IEEE Trans. Appl. Supercond*. **27**, 1601304 (2017).
22. V. Kornev, A. Sharafiev, I. Soloviev, and O. Mukhanov, *Supercond. Sci. Tech*. **27**, 115009 (2014).
23. V.K. Kornev, N.V. Kolotinskiy, A.Yu. Levochkina, and O.A. Mukhanov, *IEEE Trans. Appl. Supercond*. **27**, 1601005 (2017). doi:
24. P. Longhini, S. Berggren, A. Leese de Escobar, A. Palacios, S. Rice, B. Taylor, V. In, O.A. Mukhanov, G. Prokopenko, M. Nisenoff, E. Wong, and M.C. De Andrade, *J. Appl. Phys*. **111**, 093920 (2012).
25. V.K. Kornev, N.V. Kolotinskiy, V.A. Skripka, A.V. Sharafiev, and O.A. Mukhanov, *IEEE Trans. Appl. Supercond*. **25**, 1602005 (2015).
26. *HYPRES Nb Process Design Rules*, *Revision #24, Jan. 11* (2008) [Online]. Available: http://www.hypres.com
27. V.K. Kornev, A.V. Sharafiev, I.I. Soloviev, N.V. Kolotinskiy, and O.A. Mukhanov, *IEEE Trans. Appl. Supercond*. **26**, 1500605 (2016).
28. V.K. Kornev, A.V. Sharafiev, I.I. Soloviev, N.V. Kolotinskiy, and O.A. Mukhanov, *IEEE Trans. Appl. Supercond*. **26**, 1400104 (2016).
29. D. Gupta, D.E. Kirichenko, V.V. Dotsenko, R. Miller, S. Sarwana, A. Talalaevskii, J. Delmas, R.J. Webber, S. Govorkov, A.F. Kirichenko, I.V. Vernik, and J. Tang, *IEEE Trans. Appl. Supercond*. **21**, 883 (2011).
30. O.A. Mukhanov, D.E. Kirichenko, I.V. Vernik, T.V. Filippov, A. Kirichenko, R. Webber, V. Dotsenko, A. Talalaevskii, J.C. Tang, A. Sahu, P. Shevchenko, R. Miller, S.B. Kaplan, S. Sarwana, and D. Gupta, *IEICE Trans. Electron. E91–C*, No. 3, 306 (2008).
31. A. Leese de Escobar, O.A. Mukhanov, R. Hitt, and W. Littlefield, *IEEE Military Communications Conference, MILCOM 2006, Washington, USA, 23–25 Oct*. (2006).
32. I.V. Vernik, D.E. Kirichenko, V.V. Dotsenko, R. Miller, R.J. Webber, P. Shevchenko, A. Talalaevskii, D. Gupta, and O.A. Mukhanov, *Supercond. Sci. Tech*. **20**, S323 (2007).
33. I.V. Vernik, D.E. Kirichenko, T.V. Filippov, A. Talalaevskii, A. Sahu, A. Inamdar, A.F. Kirichenko, D. Gupta, O.A. Mukhanov, *IEEE Trans. Appl. Supercond.* **17**, 442 (2007).
34. A. Inamdar, S. Rylov, A. Talalaevskii, A. Sahu, S. Sarwana, D.E. Kirichenko, I.V. Vernik, T.V. Filippov, and D. Gupta, *IEEE Trans. Appl. Supercond*. **19**, 670 (2009).
35. D. Gupta, A. Inamdar, D.E. Kirichenko, A.M. Kadin, and O.A. Mukhanov, *Microwave Symposium Digest (MTT), IEEE MTT-S, June* (2011).
36. S. Nishijima, S. Eckroad, A. Marian, K. Choi, W.S. Kim, M. Terai, Z. Deng, J. Zheng, J. Wang, K. Umemoto, J. Du, P. Febvre, S. Keenan, O.A. Mukhanov, L.D. Cooley, C.P. Foley, W.V. Hassenzahl, and M. Izumi, *Supercond. Sci. Tech*. **26**, 113001 (2013).
37. S.A. Cybart, E.Y. Cho, T.J. Wong, V.N. Glyantsev, J.U. Huh, C.S. Yung, B.H. Moeckly, J.W. Beeman, E. Ulin-Avila, S.M. Wu, and R.C. Dynes, *Appl. Phys. Lett*. **104**, 062601 (2014).
38. S.A. Cybart, T.N. Dalichaouch, S.M. Wu, S.M. Anton, J.A. Drisko, J.M. Parker, B.D. Harteneck, and R.C. Dynes, *J. Appl. Phys.* **112**, 063911 (2012).
39. E.E. Mitchell, K.E. Hannam, J. Lazar, K.E. Leslie, C.J. Lewis, A. Grancea, S.T. Keenan, S.K.H. Lam, and C.P. Foley, *Supercond. Sci. Tech*. **29**, 06LT01 (2016).